JOURNAL OF GEOPHYSICAL RESEARCH, VOL. 91, NO. C12, PAGES 14,181–14,191, DECEMBER 15, 1986

Empirical Orthogonal Function Analyses of Tropical Atlantic Sea Surface Temperature and Wind Stress: 1964–1979

JACQUES SERVAIN

Antenne Office de la Recherche Scientifique et Technique d'Outre-Mer, Institut Français de Recherche Pour l'Exploitation de la Mer, Brest, France

DAVID M. LEGLER

Mesoscale Air-Sea Interaction Group, Department of Meteorology, Florida State University, Tallahassee

Scalar and vector empirical orthogonal function (EOF) analyses have been performed on monthly sea surface temperature (SST) and wind stress within the tropical Atlantic region for the years 1964–1979. The long-term average was subtracted from the 16-year SST and wind stress monthly fields to focus on the seasonal variability and its interannual modulations. A smaller cumulative percent of variance accounted for by the first eigenvectors of wind stress reflects the greater variability of the wind than that of SST. Analysis of regional seasonal SST events requires a combination of the first three EOFs, whereas the dominant events of the seasonal cycle of the wind stress are adequately represented by E_1 and E_2. As in the Pacific, an increase of the trade wind system is observed between the 1960s and the 1970s. Our analyses provide diagnostic insight into two types of large spacetime scale episodes. The first type is exemplified by the following sets of observations: during the spring of 1968 (spring 1976), an abnormal relaxation (intensification) of the wind stress occurred in both the northeasterlies and the southeasterlies. Subsequently, equatorially trapped anomalous warming (cooling) occurred inside the Gulf of Guinea. The second type is exemplified by the following: during 1972 to 1975, the northeasterlies (stronger) and the southeasterlies (weaker) acted out of phase, leading to a more global response of the ocean. The oceanic response was different in the northern (colder) and southern (warmer) basins.

1. INTRODUCTION

Large-scale fluctuations of the tropical ocean noticeably affect variations of climate in the low-latitude regions and can be associated with perturbations of the atmospheric circulation at higher latitudes (for the Atlantic Ocean, see as examples *Rowntree* [1976], *Hastenrath and Heller* [1977], *Markham and McLain* [1977], *Lamb* [1978], *Meehl and van Loon* [1979], and *Moura and Shukla* [1981]). Important scientific and economic interests encourage a correct understanding of the genesis and the unfolding of these dominant atmospheric and oceanic variations. The goal of the Tropical Oceans and Global Atmosphere (TOGA) program for the 10 years between 1985 and 1995 is to study the coupled ocean-atmosphere system on the time scale of several months to several years.

In the tropical regions of the oceans, large-scale dynamics appear to be wind forced. In the Atlantic the seasonal response dominates [*Merle et al.*, 1980]. In the tropical Pacific, however, the interannual signal is strongest, especially during occurrences of El Niño events [*Wyrtki*, 1975; *Leetmaa et al.*, 1983, and papers therein].

Up to this time, only a few studies have related to the interannual variability in the tropical Atlantic region. Some authors have focused on specific abnormal events. That is how, for example, 1964 and 1967 were classified as rather cool years [*Weare*, 1977; *Lamb*, 1978] inside the Gulf of Guinea, while 1963 and especially 1968 were exceptionally warm [*Weare*, 1977; *Lamb*, 1978; *Hisard*, 1980; *Merle*, 1980*a*; *Servain*, 1984]. From the results of *Hellerman* [1980] and *Perkins* [1980] based on the GARP Atlantic Tropical Experiment (GATE), it can be seen that the wind stress in summer 1974 varied from the climatological mean.

Studies within the tropical Atlantic Ocean which use data sets of several years are rare. *Weare* [1977] completed an empirical orthogonal functions (EOF) analysis with the sea surface temperature (SST) based on a data set covering the 70°N to 30°S domain (with special attention to the tropical basin) for the years 1911–1972. Some large variations having a characteristic period of a few months are depicted. However, the spatial resolution is poor (5° × 5°) and does not allow a suitable definition of the variability in some specific areas, such as the coastal and equatorial upwelling regions. *Hastenrath* [1979] found a significant coherence between the interannual signal of the sea level pressure and that of SST, but here again the spatial resolution was poor.

In anticipation of TOGA, *Picaut et al.* [1985] established a 16-year set of carefully constructed monthly SST and wind stress fields on a 2° × 2° mesh. Using this data base, *Picaut et al.* [1984] and *Servain et al.* [1985] claimed that the interannual variability is not as small as was previously believed [*Merle et al.*, 1980]. In this study, to enhance the knowledge of the variability of the tropical Atlantic region, we performed EOF analyses of that data set (a scalar method for SST, a vector method for the wind stress). We completed three different analyses for each of the two variables. In the first two analyses, the long-term average was subtracted from the SST and wind stress monthly fields to focus on the seasonal variability and its interannual modulations. Initially, the analysis covered all the available data (20°S to 30°N), but subtropical systems north of 20°N had a tendency to dominate interpretation of the results. Therefore, to

Paper number 6C0542.
0148-0227/86/006C-0542$05.00

concentrate on the equatorial region, we chose to limit the study to the area from 20°N to 20°S. In this paper we present the results of this second analysis. In order to clarify some particular points in the course of the discussion, however, we shall make occasional reference both to the first analysis and to a third, which analyzes the departures from the mean seasonal cycle.

The SST and wind stress data set and the method of analyses are discussed in the first two sections. In each of the two following sections, which present results of SST and wind stress, respectively, syntheses of seasonal and interannual variabilities are described. Finally, the results of our analyses are summarized, and the combination of variabilities of both parameters is discussed.

2. DATA

In this study we use monthly field data of SST and pseudo wind stress established by *Picaut et al.* [1985] on the tropical Atlantic region. The pseudo wind stress is defined as the magnitude of wind multiplied by its components. To obtain a dimensionally correct value of the wind stress, the components should be multiplied by an air density and a drag coefficient. *Willebrand* [1978] demonstrated that this drag coefficient can be considered constant for spectral analysis of periods greater than 10 days. Therefore the conversion to monthly wind stress means is a simple operation multiplying pseudo-stress by a suitable constant. For convenience, in this paper "wind stress" will refer to pseudo wind stress. The raw data were individual merchant ship observations for the period January 1964 through December 1979 obtained from the National Climatic Data Center, Asheville, North Carolina. Although the paucity of observations in the southern hemisphere prescribed that the study area be limited to the region north of 20°S, in spatial terms the data are denser and more uniform than those available in the tropical Pacific Ocean [*Picaut et al.*, 1985]. There were not sufficient ship observations available from before 1964 to make an accurate analysis. Therefore the time period of the study begins with January 1964 and extends through December 1979. The study includes about 2 million SST and wind observations.

In order to produce monthly regular fields on a 2° × 2° mesh, Picaut et al. used a careful combination of both subjective and objective analyses. A description of this analysis is given by *Servain et al.* [1985]. As a rule, the data density was sufficient to estimate monthly mean values of both parameters. However, during the first 7 months of 1971, there was a dramatic decrease in the number of available observations, especially in the center of the equatorial basin (Figure 1). Because of the high temporal stability of SST, this deficiency is not crucial for this parameter. However, this does not seem to be the case for wind stress; previous analyses using the original monthly mean data demonstrated that the wind stress signal was very different (more energetic) during the first half of 1971 than it was before and after this 6-month period. Such an abnormality was not noted in the SST data. In order to protect the results of these analyses from the questionable wind anomaly during the period of relatively infrequent ship observations, we chose to make another, artificial calculation of the wind stress field for each of the first 7 months of 1971 by averaging the corresponding months in 1970, 1971, and 1972. It was established that this special circumstance did not significantly influence the average wind stress field and did not induce contamination before

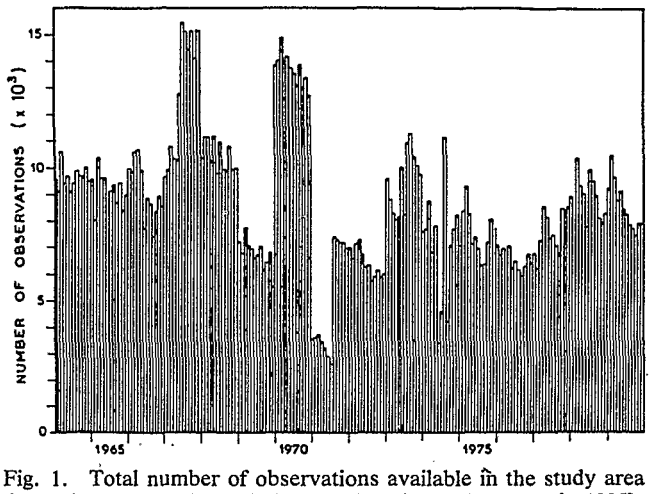

Fig. 1. Total number of observations available in the study area for each month in the period 1964–1979 [from *Picaut et al.*, 1985].

or after the first half of 1971. However, we will not make reference to the first half of 1971 when discussing the results of the wind stress analysis. Except for wind stress data from this period (January 1971 through July 1971), we used the original data sets provided by Picaut et al. for both wind stress and SST.

Descriptions of the mean seasonal cycle for SST and/or wind (or wind stress) through the tropical Atlantic domain have been largely provided in previous atlases and papers [*Hastenrath and Lamb*, 1977; *Hellerman*, 1980; *Picaut et al.*, 1985]. In this section we recall the main features of the annual signal which will be discussed later in the EOF analyses. Occasionally, we enhance the previously available information by focusing on some new elements disclosed by a careful analysis of our data set. Total monthly means (1964–1979) for both parameters are shown in Figure 2. The lowest SST appears in the eastern basin, especially in the extreme poleward parts, i.e., along the Mauritania-Senegal and Angola coasts (Figure 2*a*). For these regions, minima of SST occur during February–April in the north and during July–October in the south [*Picaut et al.*, 1985]. These minima are influenced by cold equatorward surface currents (the Canary current at the north, the Benguela current at the south) and by permanent and seasonal coastal upwellings. The mean direction of the wind stress (Figure 2*b*) is quite favorable to these upwellings during most of the year for the Mauritania and Angola coasts and from November to May for the Senegal region [*Berrit*, 1976; *Picaut et al.*, 1985].

The relatively low SST along the equator (0°–20°W) corresponds to a seasonal equatorial upwelling occurring in the boreal summer. Indirect evidence suggests this may be due to the effect of a remote forcing linked to the increase of the zonal wind stress in the western equatorial Atlantic Ocean [*Moore et al.*, 1978; *Adamec and O'Brien*, 1978; *Servain et al.*, 1982; *Busalacchi and Picaut*, 1983]. The local divergence of the wind (at its maximum in July along the equator) could also contribute to increase cooling of SST in this region [*Weisberg and Tang*, 1983; J. Servain and V. Verbeque, personal communication, 1985]. The highest SSTs are found in the western equatorial basin where the thermocline is continually deep [*Merle*, 1980*b*]. The mean seasonal position of the zonal band of maximum SST follows a similar displacement of the intertropical convergence zone

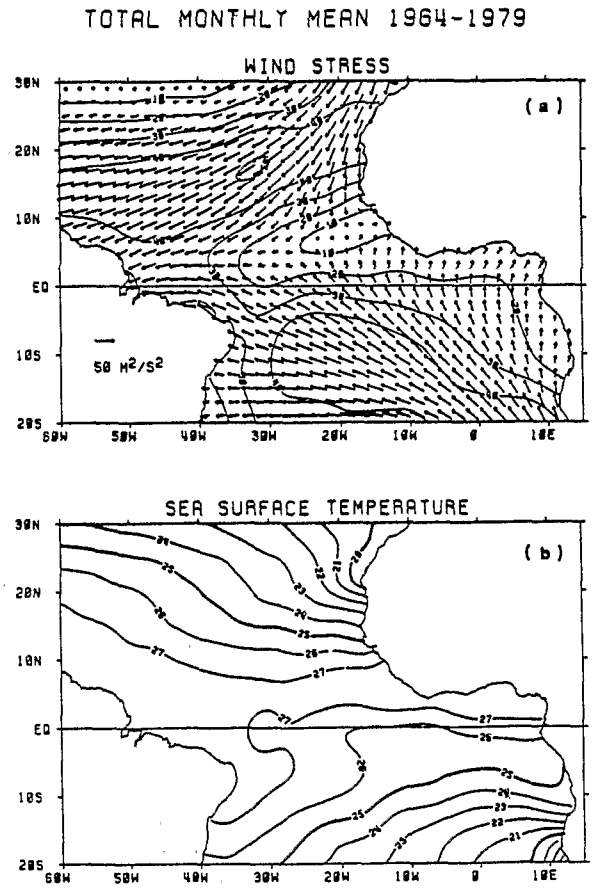

Fig. 2. Long-term averages, 1964–1979, of (*a*) wind stress and (*b*) SST. Contour intervals are 10 $m^2 s^{-2}$ and 1°C, respectively [from *Picaut et al.*, 1985].

(ITCZ), i.e., northernmost in August–September and southernmost in February–March.

The seasonal variability of the northeast trade winds is different from that of the southeast trades, as was shown by *Hellerman* [1980] and *Servain et al.* [1985]. If we check the 12 maps of the mean seasonal cycle of wind stress in the atlas of *Picaut et al.* [1985], we note that the northeast trade winds are strongest in February. At that time the wind stress magnitude is greater than 60 $m^2 s^{-2}$ for a large area centered around 10°N, 45°W. A second, smaller peak in magnitude occurs slightly further northwest in June. These northeast trades are weak from August to November and their minimum is in October–November. The magnitude of the southeast trade winds is greatest in June–July. In this case, however, wind stress magnitudes greater than 60 $m^2 s^{-2}$ are limited to the area around 10°S, 20°W. Though the monthly southeast trades are individually less energetic than the northeast trades during 7 months of the year (December to June), greater temporal stability in the broad southwesterly flow of the southern hemisphere atmospheric circulation means that both trade wind systems have a mean magnitude of the same order (Figure 2*b*). It is also interesting to note that both circulations are strong simultaneously in June, a circumstance favorable to a more dynamic response of the tropical Atlantic Ocean.

The two trade wind systems are separated by a kinematic axis extending northeastward from the western boundary to the African coast. The northernmost (8°N to 12°N) and the southernmost (2°S to 4°N) positions of the annual cycle of this ITCZ occur during the summer of their respective hemispheres.

Patterns of variance of the deviations from the SST and wind stress magnitude long-term average (1964–1979) are the combination of seasonal and interannual variability patterns calculated by *Servain et al.* [1985] on the basis of the same set of data. Regions of maximum SST variability, which occur off the African coast near Mauritania–Senegal and Angola and along the equator (0°–20°W), correspond to areas of permanent and seasonal upwellings (Figure 3*a*). The largest variance in wind stress magnitude occurs in an area straddling the mean position of the ITCZ (Figure 3*b*). Maximum variability of the wind stress direction (not shown) occurs in an area centered at 5°N, 20°W where the annual average wind stress magnitude is very small (Figure 2*b*). Furthermore, the directional variability is greatest north of 25°N, where mid-latitude atmospheric systems begin to play a dominant role.

3. METHOD

To examine spatially and temporally linked variability of SST and wind stress more fully, we chose to use empirical orthogonal functions (EOFs). This method has been detailed

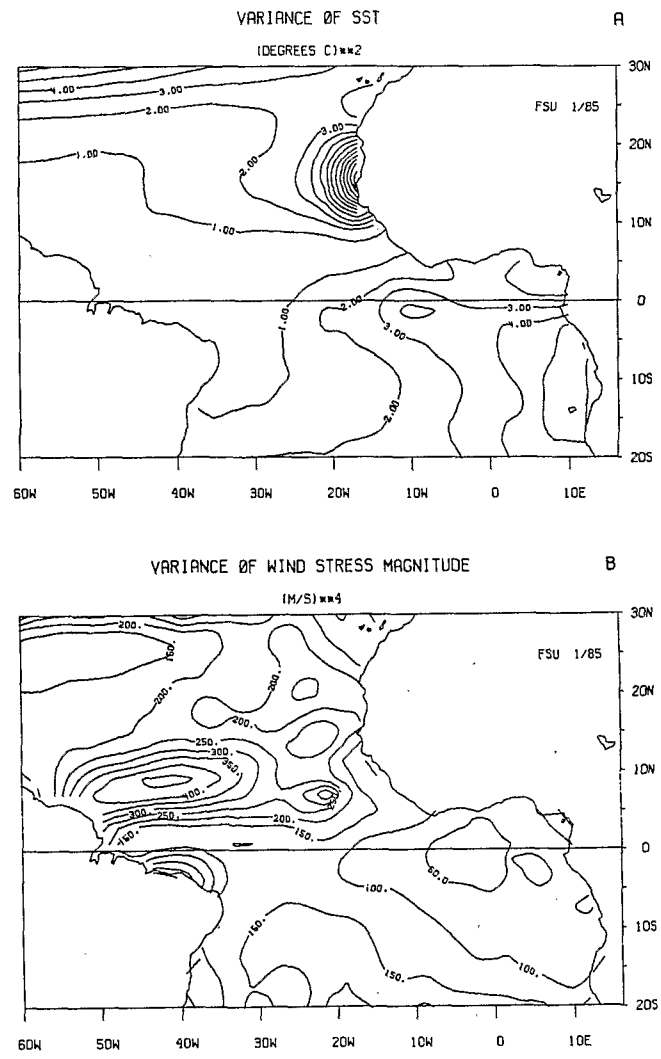

Fig. 3. Variance of (*a*) SST and (*b*) wind stress magnitude, computed with deviations from the long term means.

TABLE 1. Variance Accounted for by Eigenvectors

Parameter	Eigenvector	Percent	Cumulative Percent
Sea surface temperature	S_1	79.8	79.8
	S_2	5.8	85.6
	S_3	4.2	89.8
	S_4	1.5	91.3
Wind stress	W_1	46.6	46.6
	W_2	11.1	57.7
	W_3	4.9	62.6
	W_4	4.6	67.2
	W_5	3.2	70.4

previously in many papers [*Kundu and Allan*, 1976; *Weare*, 1977; *Legler*, 1983]. EOFs provide a series of ranked eigenvectors, each of which contains a percentage of the temporal variability of the data. Eigenvectors with the largest percentages are usually associated with physical processes. Scalar EOFs are used to analyze SST data. For the case of wind stress vector data, the zonal (u positive from the west) and meridional (v positive from the south) components were expressed as the real and imaginary parts of complex numbers respectively. An EOF analysis of these complex expressions insures that rotational variability is retained. To minimize computational and storage requirements, the W (covariance) matrix (notation of *Legler* [1983]) is formed by placing the spatial variability in rows and the temporal variability in columns. This results in covariance matrix with minimal elements [*Von Storch and Hannoschock*, 1984; *Legler*, 1984]. Therefore in this study the eigenvectors are the time series which modulate the associated coefficients: the spatial patterns.

The computed spatial patterns are oriented in some arbitrary direction determined by the orientation angle of the eigenvectors. A phase angle can be added to the spatial vectors provided that this same angle is subtracted from the associated time coefficients. Thus the spatial vectors can be rotated to lie along a meaningful direction, as long as the temporal coefficients are rotated in the opposite direction in order to insure the correct representation of the winds when reconstructing the original data. In this paper, for example, in the first EOF of wind stress, W_1, the vectors were aligned along the direction of the north-east trades.

Percents of variance for the first four eigenvectors of SST and the first five eigenvectors of wind stress are presented in Table 1. All of these EOFs are above the noise level according to selection rules presented by *Overland and Preisendorfer* [1982]. In addition, individual EOFs must be evaluated for distinctiveness (uniqueness) [see *North et al.*, 1982]. For this analysis, the first SST EOF and the first two wind stress EOFs are distinct. The uniqueness simply indicates which EOFs should be evident in a similar EOF analysis of an independent data set. While some of the EOFs discussed in this paper are not satistically distinct, they may represent physical processes; for example, we will see in the next section that SST EOFs 2 and 3 are associated with upwelling regions. The physical signatures in nondistinct EOFs cannot be considered independently significant unless they are appraised in light of the other nonunique EOFs and their magnitudes.

Each empirical orthogonal function consists of a spatial pattern modulated by an associated time series. To realize the original data at a particular time, as expressed by an individual EOF, the EOF pattern must be multiplied by the corresponding value of its associated time series. In the case of SST, the EOFs are scalar, and this realization is straightforward. Wind stress EOFs are composed of complex numbers, and thus the vector spatial patterns must be multiplied by the combination of real (a) and imaginary (b) components of the time series. That is, the magnitude of each of the spatial eigenvectors is multiplied by the magnitude (square root of $a^2 + b^2$) of the time series coefficient and the orientation of the vector arrows are rotated by the angle of the time series coefficient (arctan (b/a)). The summation of the spatial patterns multiplied by their corresponding time series results in the reproduction of the original data set. EOF analyses can therefore provide a set of basis functions representing the linked spatial and temporal variability of the data.

4. SEA SURFACE TEMPERATURE

4.1. *Seasonal Cycle*

The first eigenvector (S_1), which accounts for almost 80% of the variance of the data, primarily represents the seasonal cycle. Because so much of the variance is contained in the seasonal cycle, the pattern of eigenvector 1 (Figure 4*a*) is very close to that of SST variance already shown in Figure 3*a*. It is more detailed than but quite similar to the tropical Atlantic region of the S_1 pattern previously computed by *Weare* [1977] in which the spatial grid was only 5° × 5°. In Weare's paper the percent of variance is 84.6, but the study area was larger than ours, covering the northern Atlantic mid-latitudes (30°S to 70°N; 20°E to 100°W). In the present

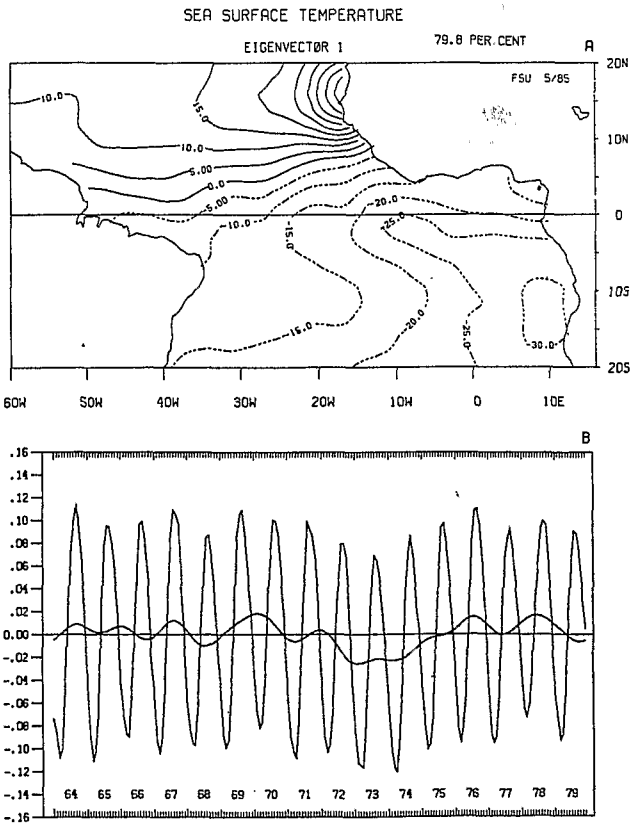

Fig. 4. (*a*) SST eigenvector 1 spatial pattern and (*b*) its associated time series. The contour interval of the isotherms is 5°C. The low-frequency curve is the result of a low-pass filter (>12 months).

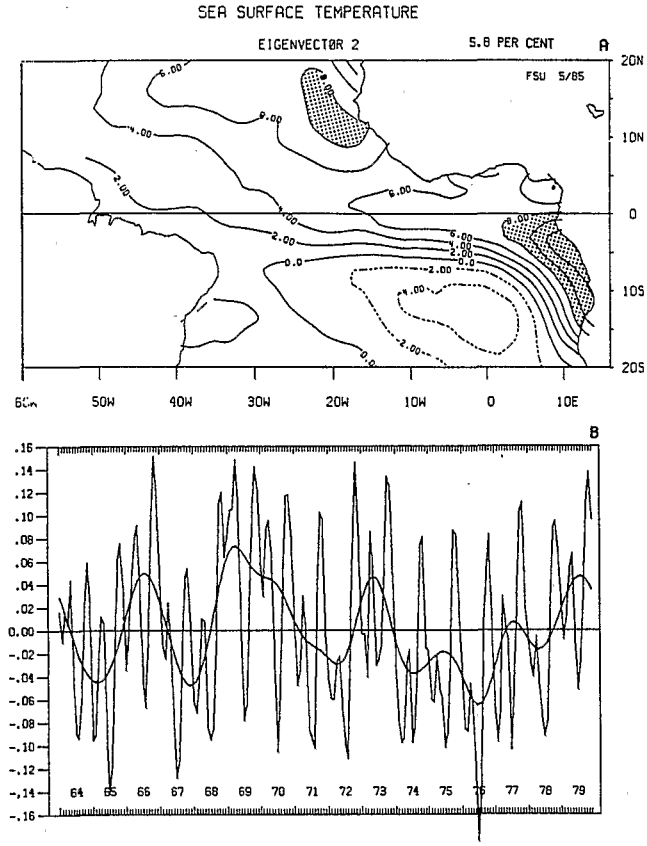

Fig. 5. Same as Figure 4, except for eigenvector 2; the contour interval is 2°C. Shaded areas indicate magnitudes greater than 8°C.

study, if we use the 30°N to 20°S region, the percent of variance of S_1 increases to 81.2%. The seasonal climatic balance between the two hemispheres is well conveyed by opposite sign patterns on both sides of the thermal equator. On the corresponding time series (Figure 4*b*), positive (negative) peaks occur during boreal (austral) summers.

Spatial and temporal distributions of S_2 (Figure 5) and S_3 (Figure 6) are more complicated. They approach the description of features with smaller scale, particularly the seasonal upwelling events. Eigenvector 2, which represents 5.8% of the variance, is in phase in most of the tropical Atlantic ocean (Figure 5*a*). The only out-of-phase region is located in the south central basin. There are two areas of important positive values. The first one is largely spread off the Senegal coast, and the second is trapped along the equator (close to 10°W) and the south and north coasts of the Guinea Gulf. This pattern reveals a double influence: the seasonality of the two hemispheres and the seasonal upwelling system in the tropical Atlantic Ocean. A combination of a semiannual and a weaker annual signal is noted on the corresponding time series (Figure 5*b*). Two sets of main peaks regularly separated in time, a negative one in July and a positive one in November, are linked to the increase of seasonal cooling inside the Gulf of Guinea and the end of the warm season along the Senegal coast, respectively. Two other sets of peaks, with weaker amplitudes than the first, occur in April (positive) and in February (negative). The April maximum corresponds to the time when warming is greatest inside the Gulf of Guinea. The February peak reflects the reinforcement of the seasonal coastal upwelling in the Senegal oceanic region and the winter cooling in the northern hemisphere.

Eigenvector 3 (4.2% of the variance) indicates the out-of-phase variability of the equatorial and south coastally trapped pattern and the Senegal coastal region (Figure 6*a*). This is in contrast to S_2, where the in-phase relationship of these two regions is described. In the southern area of the basin, also out of phase with the equatorial and south-coastal pattern, is another patch of maximum variability. The configuration of this southernmost patch (centered by 5°S, 18°W) has a striking likeness with the phase pattern associated with the annual signal in this region [*Merabet*, 1983]. The northern maximum near Senegal represents the seasonal upwelling. An annual signal dominates the S_3 time series (Figure 6*b*), where the range of monthly values is not the same order of the preceding eigenvector. Onset of the strong seasonal upwelling which appears along the Senegal coast is noted as negative peaks occurring each January. The positive peaks (arising principally in June) correspond both to the beginning of the warm season in the Senegal oceanic region and of the cold season along the southern coast of the Gulf of Guinea, and to the end of the warm season in the central basin south of the equator.

4.2. *Interannual Variability*

The S_1 pattern and time series for SST (Figure 4) are clear in their representation of variations of the annual signal. These variations, as depicted by the Fourier wave low-pass filter (>12 months), are less substantial during the first 5 years of the study period than during the following years.

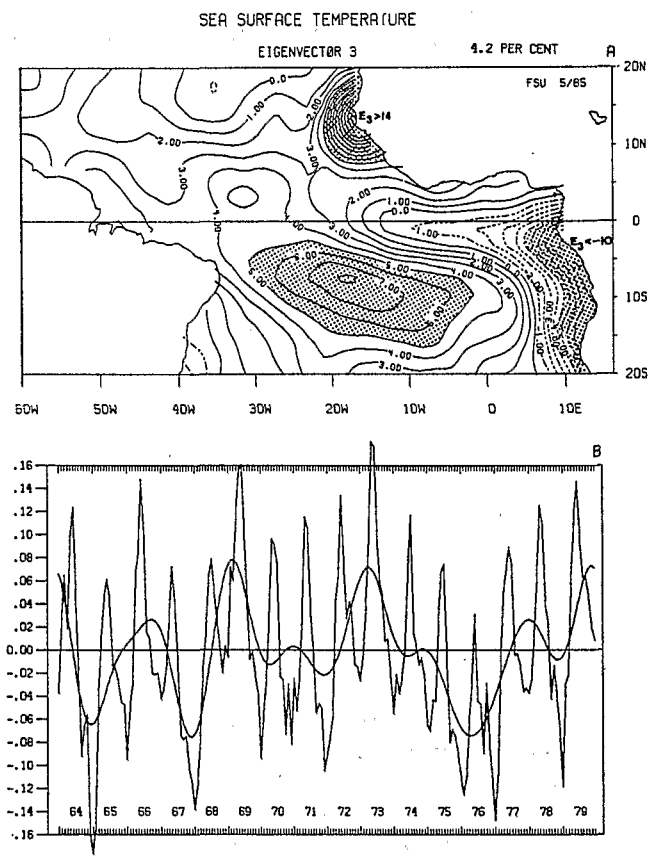

Fig. 6. Same as Figure 4, except for eigenvector 3; the contour interval is 1°C. Shaded areas indicate magnitudes greater than 5°C.

From 1972 to 1975 the SST in the northern (southern) hemisphere was abnormally cold (warm). During this period the magnitude of the anomaly which appears in S_1 is about −0.3°C in the north and + 0.4°C in the south, resulting in an anomalous difference between them of about 0.7°C. Inverse episodes smaller in both magnitude and phase are noticed in 1969–1970 and 1978.

The patterns of S_2 and S_3 (Figures 5*a* and 6*a*) are in phase in the northern and southwestern regions, as are their low-frequency signals (Figures 5*b* and 6*b*). Therefore, for a large part of the basin, these two eigenvectors are associated with the same long-term variability. The unfiltered time coefficients of S_2 and S_3 are by definition uncorrelated, but they can both describe different aspects of the same physical process, thus enabling their filtered time series coefficients to be correlated. The low-frequency signal of S_2 and S_3 clearly shows some large-scale anomalous events with periods of 3 to 4 years. For example, the most prominent contributions by S_2 and S_3 are the warming (≈ +0.6°C) in 1969 and the cooling (≈ −0.4°C) during 1976, which covered the areas where the additive spatial patterns (Figures 5*a* and 6*a*) are positive, i.e., off the Senegal coast and, to a lesser extent, the region north of the equator and the eastern equatorial region. A more detailed examination of the results can disclose some interesting features with regard to interannual variabilities. As exemplified, it is interesting to note that during the first half (1972–1973) of the large warming episode as denoted in S_1 in the south and equatorial regions, the S_2 summertime negative peak was a month late in both 1971 and 1972 and was absent in 1973. By contrast, it was very prominent in 1976. Furthermore, the oversize maxima arising in January 1965 and in May–June 1973 on the S_3 time series are principally related to premature upwelling and premature warming along the Senegal coast.

The combination of all three SST EOFs yields the major events during this time period. At the end of 1964 and again in 1967, there was a general cooling over most of the Atlantic, particularly where seasonal upwelling was strong. Likewise, in 1966 there is a lesser warming in these same areas. The early months of 1969 are revealed as being warmer, but in middle to late 1969 and extending into 1970, the combination of S_1 and S_2 dominates and depicts warming in the north and cooling in the south Atlantic. During the years 1972–1976 there was a cooling in the north (~−0.90°C) and a warming in the south (+0.7°C) except in 1973, when the warming in the Gulf of Guinea and off the coast of Senegal was unusually strong.

The magnitude of the contribution to the seasonal and interannual variability by EOFs higher than S_3 are much smaller than those of the previously discussed EOFs and will not be discussed here.

5. WIND STRESS

5.1. *Seasonal Cycle*

For this study area (with a northern limit at 20°N), the variance accounted for by eigenvector 1 (46.6%) is noticeably larger than in the case where the northern limit is 30°N (36%). This difference is explained by the fact that the W_1 pattern collects all the variability in the ITCZ rather than further north (compare Figure 7*a* with Figure 3*b*). Eigenvector 1 is similar to a previous study established by *Legler* [1983] on the Pacific region, using the same limits (20°N to 20°S). Since the seasonal variability is larger in the tropical Atlantic region than in the corresponding area of the Pacific [*Philander*, 1979; *Merle et al.*, 1980; *Busalacchi and O'Brien*, 1981], it is not surprising that the amount of variance explained by eigenvector 1 is greater in the Atlantic case (46.6% versus 35.4%).

Recall from the discussion of the method that there are two components of the modulating time series, real and imaginary. If either of these components is negligible, then the spatial vectors have little rotational variability in time. For relatively small imaginary components, the vectors simply oscillate along the axis of the vector with positive and negative values. For small real component values, the vectors tend to oscillate along a line perpendicular to the vector orientation. For the time series with equal magnitudes of real and imaginary parts, the temporal variability of the spatial vectors is spread over many rotation angles. Predominance of the real component which fluctuates from negative to positive in the W_1 time series (Figures 7*b* and 7*c*) indicates a 180° rotation of the W_1 pattern. For both tropical regions the W_1 time series principally represents the annual signal with a greatest magnitude of the trade winds during the winters of their respective hemispheres.

We saw previously (Figure 2*b*) that total monthly mean magnitudes for both the Atlantic trade systems are similar. In this EOF analysis, however, the pattern of W_1 is latitudinaly asymmetric in the same fashion as the variance of the wind stress magnitude (Figure 3*b*). Since almost half of the signal of the original data can be reconstructed by a combination of the W_1 pattern and its corresponding time series, it is not surprising, as is depicted primarily by the real component (Figure 7*b*) that a 1.5 higher range in the negative values than in the positive ones normalizes the magnitude of the northeasterlies when the southeasterlies are maximal. Conversely, when the northeasterlies are strong (positive values), smaller amplitudes of the real component time series correctly reproduce the wind stress vectors in the W_1 pattern.

An amplitude rotation analysis (Figures 7*d* and 7*e*) indicates that the W_1 wind stress field rotates 180° clockwise during a short period in November–December. A rotation in the opposite direction occurs more slowly about May–July. By contrast, a period of steadiness occurs from December to May and from June–July to October–November, indicating sustained northeasterly and southeasterly trade wind periods.

As opposed to W_1, the explained variance of W_2 in the 20°N to 20°S region (11.1%) is less than that of a similar EOF analysis in the 30°N to 20°S domain (17%). While W_1 collects most of the variability in the trade wind zones, W_2 chiefly describes the western subtropical regions, both in phase (Figure 8*a*). The associated time series contains annual and semiannual signals. The large annual cycle clearly appears on the W_2 real component with a similar range for both positive and negative values (Figure 8*b*).

The wind stress vector magnitudes of W_3 pattern (only 4.9% of the variance) are weaker and more spatially uniform than the first two eigenvectors (Figure 9*a*). Relatively larger variabilities are found in the middle of the south tropical Atlantic region and in the western part of the equatorial region. Moreover, the time series of the real and imaginary components (Figures 9*b* and 9*c*) are noisier than preceding eigenvectors.

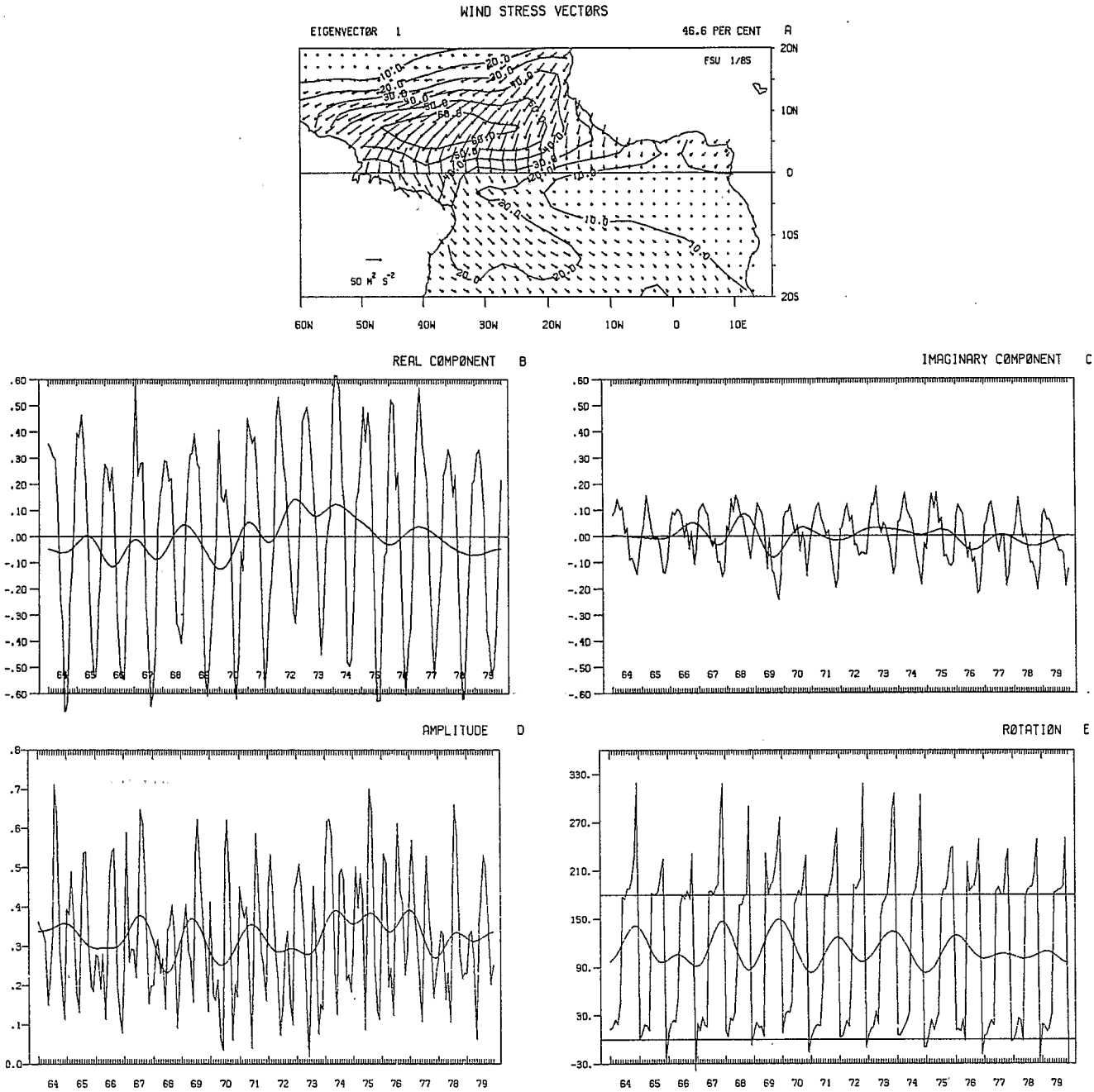

Fig. 7. (*a*) Wind stress eigenvector 1 spatial pattern and the (*b*) real and (*c*) imaginary parts of the associated time series. The contour interval of the isotachs is 10 m^2 s^{-2}. The low-frequency curve is the result of a low-pass filter (>12 months). Associated time series are expressed as (*d*) amplitude and (*e*) rotation. Rotation is in degrees counterclockwise to the orientation of the spatial pattern vectors.

5.2. *Interannual Variability*

A careful examination of enlargements of the W_1 time series (Figures 7*b* and 7*e*) discloses that in the beginning of the 1970s the directional stability of the southeasterly trades occurred only in July–October and the wind stress magnitude was weaker. During the same period the northeast trades had a longer duration and were anomalously strong. The deducible positive long-term anomaly ($\approx$ 3–5 m^2 s^{-2}) is obvious in the low-frequency curves of the W_1 real and imaginary components (Figures 7*b* and 7*c*). Another exceptional time period during the 1968 and 1969 years includes three weakenings of the sustained trade wind system (two for northeast trades and one for southeast trades). This 1968 even was discussed previously by some authors as linked to an abnormal southward displacement of the ITCZ [*Lamb*, 1978; *Hisard*, 1980; *Merle*, 1980*a*].

The variability of the wind stress in the western subtropical regions, as indicated primarily by the real component of W_2 (Figure 8*b*), is strongly different in the course of the years 1964–1979. A set of negative peaks arises almost regularly in November–December during the 1960s and disappears after 1969. A second set of positive peaks indicating strong northeasterlies in the northwest portion of the tropical Atlantic occur systematically about the month of June during the 1970s, whereas they are generally weak or absent in

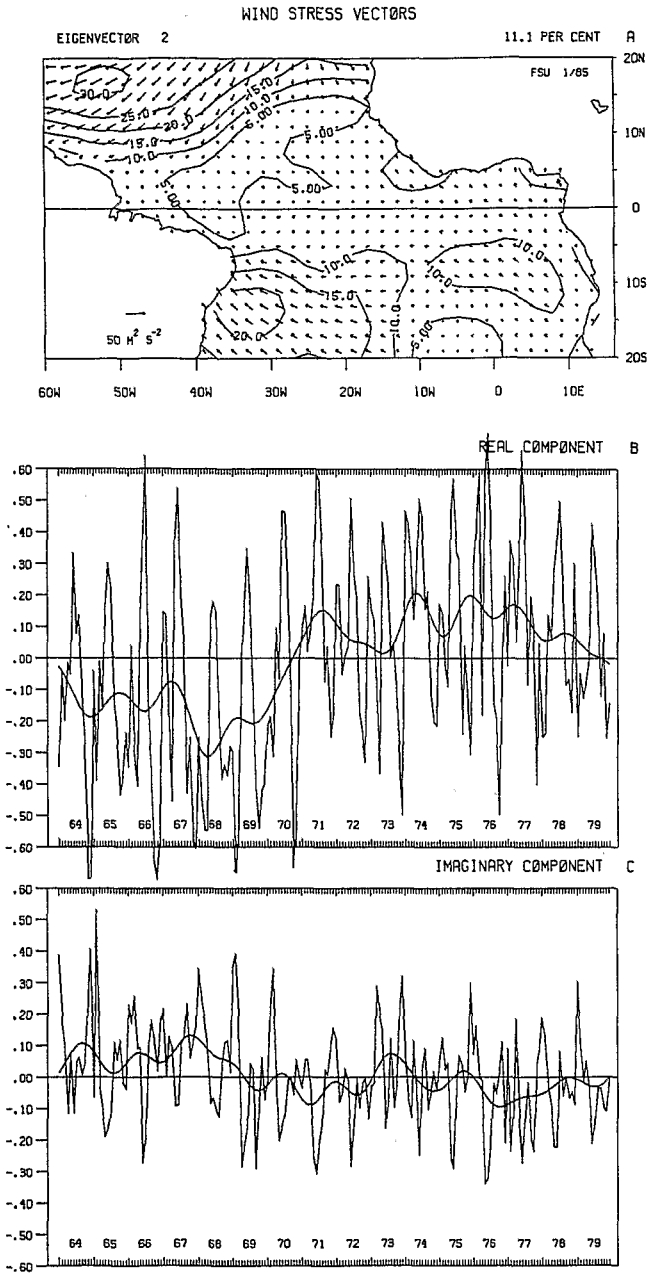

Fig. 8. Same as Figure 7, except for eigenvector 2; the contour interval is 5 m^2 s^{-2}.

preceding years. This perturbation also occurs in June in the mean seasonal cycle computed from the 1964–1979 data set by *Picaut et al.* [1985]. This secondary seasonal event seems valid because a similar one is also depicted by *Hastenrath and Lamb* [1977], who used the 60 years of observations before 1971.

The amplitude rotation analysis of W_2 (not shown) indicates that the mean orientation of the associated pattern (Figure 8*a*) is about 130° counterclockwise during the 1960s and about 80° counterclockwise during the 1970s. Thus the northwestern (southwestern) subtropical wind stress circulation turned consequently more southward (westward), corresponding to a net strengthening of the trade system throughout the study time period. This substantial long-term trend amplified by weakened magnitudes in November–December during the 1960s and increased magnitudes in June during the 1970s is observed in the low-frequency curve of the W_2 time series (Figures 8*b* and 8*c*). A similar change between the 1960s and the 1970s has been recognized by *Legler* [1983] for the tropical Pacific Ocean. In order to investigate these Atlantic features fully, we checked the monthly basic data minus the 16-year long-term average over the total available domain, 20°S to 30°N. In the northwest region, one important cyclonic wind stress perturbation (associated with a decrease of the northeast trades) was present during the winters of the 1960s. This circulation was very weak or absent during this same season of the subsequent 10-year period.

In the southwest region, we noted in the monthly means an important decrease of southeasterlies in Novem-

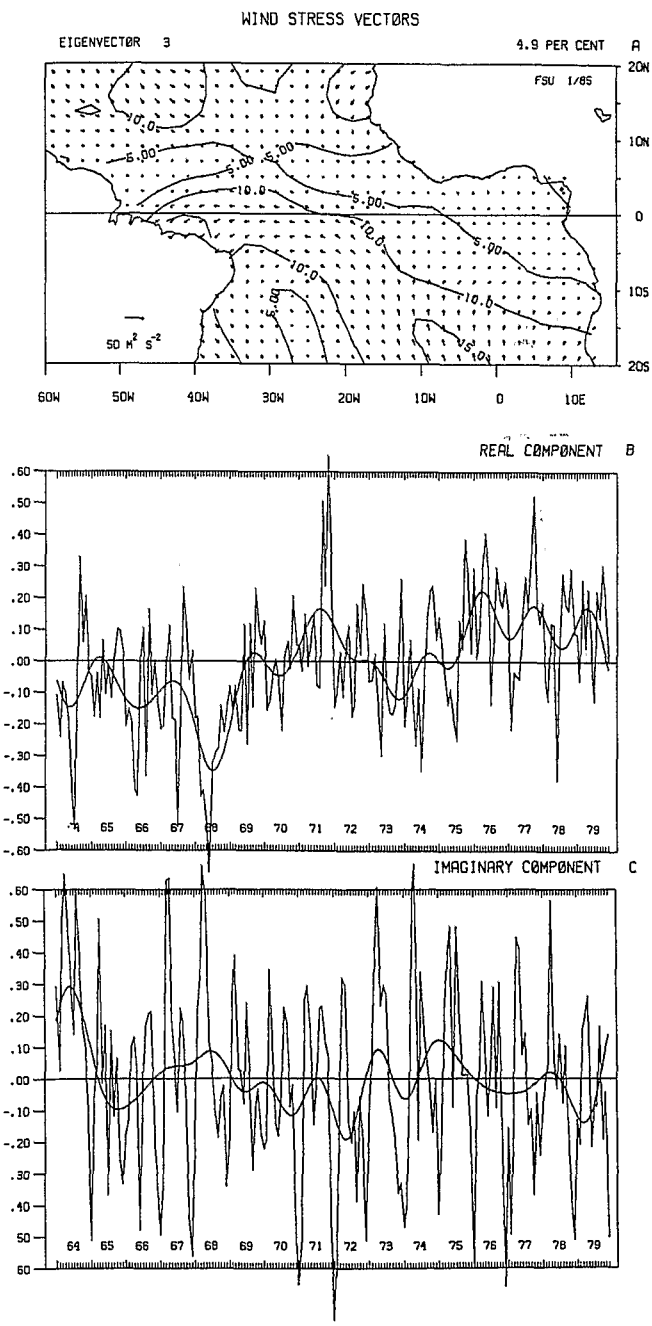

Fig. 9. Same as Figure 7, except for eigenvector 3; and the contour interval is 5 m^2 s^{-2}.

ber–December 1967 that corresponded to the onset of the considerable weakening of the trade winds denoted previously by eigenvector 1 for the years 1968–1969. A careful check of W_3 real and imaginary components (Figures 9*b* and 9*c*) and of their corresponding amplitude rotation time series (not shown) reveals only one distinctive event in the course of the years 1964–1979 which was of long duration and was both great in magnitude and steady direction. This event took place between April and June 1968 and corresponded to an approximately 10 m^2 s^{-2} magnitude in the opposite direction of the W_3 wind stress pattern. After 1973 the W_3 pattern rotated clockwise about 90° and signified increased northeast trades in the western equatorial region.

Although wind stress eigenvectors W_4 and W_5 (not shown) are above the noise level, their interpretation is difficult, especially that of W_5. W_4 indicates a weakening (~1.4 m^2 s^{-2}) of the southeast trades centered at 20°W, 17°S, during July–December 1967. Although smaller, it complements the large decrease already depicted in W_1 and W_2. Conversely, in late 1975 and early 1976 there is a small amplification of the southeast trades in this region. Additionally, a long-term trend in the time series corresponds to a small increase in these trades, although this too is better depicted in W_2.

6. Summary and Discussion

The cumulative percent of variance accounted for by the first three eigenvectors is considerably smaller for wind stress than for SST (62.6 and 89.8, respectively). This reflects the larger variability of the atmospheric circulation compared to that of SST. The wind stress cumulative percent is nevertheless greater than that for the Pacific, where *Legler* [1983] found 47% for the first three eigenvectors. Once more, a prominent seasonal signal in the tropical Atlantic region is the cause of increase of the variance accounted for by the first eigenvectors.

The SST large-scale seasonal cycle of both the thermal hemispheres is well described by S_1. However, a combination of the first three EOFs is needed to analyze the regional seasonal events. Such is the case for the seasonal upwelling along the Senegal coast. S_1 (and to a smaller extent S_2) indicates that this event is strongest in February–March, when the seasonal cooling of the northern hemisphere develops. The beginning of this cooling in January is clearly represented by S_3. Most of the duration of the subsequent warm season (in the course of the boreal summer) is well accounted for by S_1; its onset in June and its conclusion in November are illustrated by S_3 and S_2, respectively.

The strong seasonal signal of SST inside the Gulf of Guinea appears clearly in each of the three first eigenvectors. In June, S_3 depicts the beginning of the cold season along the southern coast of the Gulf of Guinea. The onset in July of the equatorial and northcoastal upwellings (from Ivory Coast to Nigeria) are well described by S_2. For this month and the two subsequent months, S_1 depicts a more large scale cooling in the southern portion of the Gulf of Guinea. In the equatorial and southern domains of this gulf, the subsequent warming period is mainly denoted by S_1 during the austral summer. For the equatorial region the highest temperatures of this warm season (in April) are further related by S_2.

The dominant events of the seasonal cycle of the wind stress are well represented by W_1 and W_2. W_1 is principally annual and describes mainly the two trade wind systems with a preference for the northeast trades, where a maximum of variability is due to the seasonal migration of ITCZ. W_1 indicates that the rotation occurring in November–December, linked to the increase of the northeast trades, is generally quicker than the opposite turning in May–July which precedes the greatest magnitude of the southeast trades. W_2, chiefly influenced by the wind stress variability in the western subtropical areas (particularly in the north), describes annual and semiannual perturbations in these regions. The W_2 annual signals are linked to both sustained trade winds during their respective hemispheric winters, and the W_2 semiannual signal corresponds principally to the secondary maximum of northeast trades occurring about June in the northwest subtropical regions.

Our EOF analysis provides insight into significant anomalous episodes with large space and time scales which developed in the tropical Atlantic region during the years 1964–1979. The results presented here complete, detail, and amplify those previously developed by *Weare* [1977], who used solely the SST data for the period 1911–1972.

The reversal of the trade winds along the equator during May–June 1968 near 30°W [*Servain*, 1984] is adequately depicted by the third eigenvector of the EOF analysis. This reversal is unique for the 16-year period at this longitude [*Picaut et al.*, 1984]. W_1 and W_2 show that this dramatic event took place at the midpoint of a vast episode extending throughout the entire tropical region from the fall of 1967 through the spring of 1969. During this period the wind stress was weaker than normal for both north and south trade systems. *Servain* [1984] noted as did *Picaut et al.* [1984] that this reversal of the trade winds preceded an extremely anomalous warm episode of SST in the Gulf of Guinea: the large positive deviations of SST from the mean year [*Lamb*, 1978; *Merle*, 1980*b*; *Hisard*, 1980] were equatorially trapped [*Servain*, 1984; *Picaut et al.*, 1985]. The weak succeeding upwelling was limited to August only. Our EOF analysis, computed with the basic data minus the long-term average, cannot accurately explicate the extension of the warming season and the subsequent shorter and smaller equatorial upwelling in the first eigenvectors, especially for SST in 1968. A shift in the SST seasonal signal is better supported by an EOF analysis of the monthly deviations from the mean seasonal cycle. In such an EOF analysis (not shown) we found more evidence of the 1968 SST event.

In direct contrast to the 1968 event, the seasonal equatorial upwelling was stronger than usual during the summer of 1976. An exceptional cold departure of SST from the long-term average (more than 5°C in August) and its location further east than the inverse case of 1968 are undoubtedly responsible for the greater depiction of this event by the EOF analysis presented here (see Figure 5*b*). During the preceding months there was a simultaneous intensification of the northeast and southeast trades [*Picaut et al.*, 1985]. An anomalous increase of the western equatorial easterlies in June 1976 (more than 30 m^2 s^{-2} for the monthly anomaly) resulted from this strengthened convergence. For the mean June the wind stress is this region is weaker than the long term average. Consequently, for the wind stress the 1976 equatorial event appears more prominent in our EOF analysis of the monthly anomalies.

Another large-scale episode, mainly represented by the first eigenvector of each parameter, occurred in the tropical Atlantic region during the beginning of the 1970s. The

northern and the southern hemispheres opposed each other, in contrast to the 1968 and 1976 events in which the whole tropical basin acted in phase. From the beginning of 1972 through the end of 1975, the north (south) basin was generally colder (warmer), except in 1973, when the Gulf of Guinea and the waters off the coast of Senegal were unusually warm, while the northeasterlies (southeasterlies) were, overall, stronger and longer (weaker and shorter) than normal. The northern magnification of the wind stress is also due to a western subtropical system more anticyclonic than that in the 1960s.

The north-south dipole for the SST long-term anomaly in 1972–1975 is not exceptional [*Hastenrath and Heller*, 1977; *Moura and Skukla*, 1981] and is also observed (in S_1) with the opposite sign during the years 1969–1970. This dipole is confirmed by S_2 and S_3 (warming in the north and along the eastern equator; cooling in the south, particularly in 1970).

A correlation analysis was performed between the monthly anomalies time series components of SST and wind stress (amplitude in the case of the wind stress). Despite the difference of variances accounted for by eigenvector 1 of the wind stress (46.6%) and SST (79.8%), wind stress leads SST by 1 month with a correlation coefficient of 0.45 (0.83 for the low-frequency signal). In conclusion, this relation corroborates that some of the interannual variability of the SST annual signal in the eastern tropical Atlantic Ocean is directly connected to a large amount of interannual variability of the annual signal of the wind stress in the western region at similar time scales. For SST, the second and third eigenvectors are associated with coastal and equatorial seasonal upwellings. These eigenvectors unite to explain semiannual and other perturbations to the annual signals. W_2 of the wind stress illustrates the main variability in the western subtropical regions, and W_3 represents the easterlies fluctuations in the western equatorial region. However, outside the equatorial strip where the equatorial trapped events are correctly depicted by eigenvectors of superior rank, the accuracy of our analyses is limited to a study of a global response between wind stress and SST. Further investigations, as for example the use of the curl of the wind stress and EOFs in the frequency domain, would be able to contribute to a finer description of the response.

Acknowledgments. We would like to thank Jim O'Brien and Tony Busalacchi for comments and helpful discussions during this research. In addition, thanks to Helen McKelder and Rita Kuyper who cheerfully typed the manuscript and to all those responsible for producing the original data set. Support for D.M.L. was provided under NSF grant OCE-8119052 and NOAA grant NA83AA-D-00024. In addition, J.S. acknowledges support by Centre National pour l'Exploitation des Oceans contract 84-3149, IFREMER contract 85-1-430503 and Centre National de la Recherche Scientifique grant 91-0712, and ORSTOM. We sincerely appreciate this support.

REFERENCES

Adamec, D., and J. J. O'Brien, The seasonal upwelling in the Gulf of Guinea due to remote forcing, *J. Phys. Oceanogr.*, *8*, 1050–1060, 1978.

Berrit, G. R., Les eaux froides côtières du Gabon à l'Angola sont-elles dues à un upwelling d'Ekman? *Cah. ORSTOM, Ser. Oceanogr.*, *14*, 273–278, 1976.

Busalacchi, A. J., and J. J. O'Brien, Interannual variability of the equatorial Pacific in the 1960's, *J. Geophys. Res.*, *86*, 10,901–10,907, 1981.

Busalacchi, A. J.,and J. Picaut, Seasonal variability from a model of the tropical Atlantic Ocean, *J. Phys. Oceanogr.*, *13*, 1564–1588, 1983.

Hastenrath, S., On modes of tropical circulation and climate anomalies, *J. Atmos. Sci.*, *35*, 2222–2231, 1979.

Hastenrath, S., and L. Heller, Dynamics of climate hazards in northeast Brazil, *Q. J. R. Meteorol. Soc.*, *103*, 77–92, 1977.

Hastenrath, S., and P. J. Lamb, *Climatic Atlas of the Tropical Atlantic and Eastern Pacific Oceans*, University of Wisconsin Press, 112 pp, Madison, 1977.

Hellerman, S., Charts of the variability of the wind stress over the tropical Atlantic, *Deep Sea Res.*, *26*, GATE suppl. II, 63–75, 1980.

Hisard, P., Observation de réponse de type "El Niño" dans l'Atlantique tropical oriental Golfe de Guinée, *Oceanol. Acta.*, *3*, 69–78, 1980.

Kundu, P. K., and J. S. Allan, Some three dimensional characteristics of low-frequency current fluctuations near the Oregon coast, *J. Phys. Oceanogr.*, *6*, 181–199, 1976.

Lamb, P. J., Case studies of tropical Atlantic surface circulation pattern during recent sub-Sahara weather anomalies, 1967–1968, *Mon. Weather Rev.*, *106*, 282–291, 1978.

Leetmaa, A., et al., Papers from 1982/83 El Niño/Southern Oscillation Workshop, 229 pp., Atl. Oceanogr. and Meteorol. Lab., Natl. Ocean. and Atmos. Admin., Miami, Fla., 1983.

Legler, D. M., Empirical orthogonal function analysis of wind vectors over the tropical Pacific region, *Bull. Am. Meteorol. Soc.*, *64*, 234–241, 1983.

Legler, D. M., Response to "Comments on empirical orthogonal function analysis of wind vectors over the tropical Pacific region," *Bull. Am. Meteorol. Soc.*, *65*, 162, 1984.

Markham, C. G., and D. R. McLain, Sea surface temperature related to rain in Ceara, northeastern Brazil, *Nature*, *265*, 320–323, 1977.

Meehl, G. A., and H. van Loon, The seesaw in winter temperatures between Greenland and northern Europe, III, Teleconnections with lower latitudes, *Mon. Weather Rev.*, *107*, 1095–1106, 1979.

Merabet, N., Analyse du cycle saisonnier moyen de la température de surface de l'atlantique tropical, rapport D.E.A., 97 pp., Univ. de Bretagne Occident., Brest, France, 1983.

Merle, J., Variabilité thermique annuelle et interannuelle de l'océan Atlantique equatorial est, L'hypothèse d'un "El Niño" Atlantique, *Oceanol. Acta.*, *3*, 209–220, 1980*a*.

Merle, J., Seasonal heat budget in the equatorial Atlantic, *J. Phys. Oceanogr.*, *10*, 464–469, 1980*b*.

Merle, J., M. Fieux, and P. Hisard, Annual signal and interannual anomalies of sea surface temperature in the eastern equatorial Atlantic, *Deep Sea Res.*, *26*, GATE suppl. II, 77–101, 1980.

Moore, D. W., P. Hisard, J. P. McCreary, J. Merle, J. J. O'Brien, J. Picaut, J. M. Verstraete, and C. Wunsch, Equatorial adjustment in the eastern Atlantic, *Geophys. Res. Lett.*, *5*, 637–640, 1978.

Moura, A. D., and J. Shukla, On the dynamics of droughts in northeast Brazil: Observations, theory and numerical experiments with a general circulation model, *J. Atmos. Sci.*, *38*, 2653–2675, 1981.

North, G. R., T. L. Bell, and R. F. Cahalan, Sampling errors in the estimation of empirical orthogonal functions, *Mon. Weather Rev.*, *110*, 699–706, 1982.

Overland, J. E., and R. W. Preisendorfer, A significance test for principal components applied to a cyclone climatology, *Mon. Weather Rev.*, *110*, 1–4, 1982.

Perkins, H., Low frequency forcing of the tropical Atlantic ocean under the ITCZ during GATE, *Deep Sea Res.*, *26*, GATE suppl. I, 225–236, 1980.

Philander, S. G. H., Variability of the tropical oceans, *Dyn. Atmos. Oceans*, *3*, 191–208, 1979.

Picaut, J., J. Servain, A. J. Busalacchi, and M. Seva, Interannual variability versus seasonal variability in the tropical Atlantic, *Geophys. Res. Lett.*, *11*, 787–790, 1984.

Picaut, J., J. Servain, P. Lecomte, M. Seva, S. Lukas, and G. Rougier, *Climatic Atlas of the Tropical Atlantic Wind Stress and Sea Surface Temperature 1964–1979*, 467 pp., University of Hawaii, Honolulu, 1985.

Rowntree, P. R., Response of the atmosphere to a tropical Atlantic Ocean temperature anomaly, *Q. J. R. Meteorol. Soc.*, *102*, 607–625, 1976.

Servain, J., Réponse océanique à des actions éloignées du vent dans

le Golfe de Guinée en 1967–1968, *Oceanol. Acta*, *7*, 297–307, 1984.

Servain, J., J. Picaut, and J. Merle, Evidence of remote forcing in the equatorial Atlantic Ocean, *J. Phys. Oceanogr.*, 2, 457–463, 1982.

Servain, J., J. Picaut, and A. J. Busalacchi, Interannual and seasonal variability of the tropical Atlantic Ocean depicted by sixteen years of sea-surface temperature and wind stress, in *Coupled Ocean-Atmosphere Models*, pp. 211–237, edited by J. C. J. Nihoul, Elsevier, New York 1985.

Von Storch, H., and G. Hannoschock, Comments on "Empirical orthogonal function analysis of wind vectors over the tropical Pacific region," *Bull. Am. Meteorol. Soc.*, *65*, 162, 1984.

Weare, B. C., Empirical orthogonal analysis of Atlantic Ocean surface temperature, *Q. J. R. Meteorol. Soc.*, *103*, 467–478, 1977.

Weisberg, R. H., and T. Y. Tang, Equatorial ocean response to growing and moving wind systems with application to the Atlantic, *J. Mar. Res.*, *41*, 461–486, 1983.

Willebrand, J., Temporal and spatial scales of the wind field over the North Pacific and North Atlantic, *J. Phys. Oceanogr.*, *8*, 1080–1094, 1978.

Wyrtki, K., El Niño—The dynamic response of the equatorial Pacific Ocean to atmospheric forcing, *J. Phys. Oceanogr.*, *5*, 572–584, 1975.

D. M. Legler, Department of Meteorology, Meteorology Annex, Florida State University, 435 OSB, Tallahassee, FL 32306.

J. Servain, Antenne ORSTOM, Institut Français de Recherche pour l'Exploitation de la Mer, B. P. 337, 29273 Brest Cedex, France.

(Received March 12, 1986;
accepted May 6, 1986.)